LA-UR- 08-6010

Approved for public release;
distribution is unlimited.

Title:	A theory of jet shapes and cross sections: from hadrons to nuclei
Author(s):	Ivan Vitev, T-16 Simon Wicks, Columbia Univ. Benwei Zhang, T-16
Intended for:	Physical Review D or Journal of High Energy Physics

Form 836 (7/06)

A theory of jet shapes and cross sections: from hadrons to nuclei

Ivan Vitev,[1] Simon Wicks,[2] and Ben-Wei Zhang[1,3]

[1] *Los Alamos National Laboratory, Theoretical Division, MS B238, Los Alamos, NM 87545, USA*
[2] *Department of Physics, Columbia University, 538 West 120-th Street, New York, NY 10027, USA*
[3] *Institute of Particle Physics, Hua-Zhong Normal University, Wuhan, 430079, China*

(Dated: September 5, 2008)

For jets, with great power comes great opportunity. The unprecedented center of mass energies available at the LHC open new windows on the QGP: we demonstrate that jet shape and jet cross section measurements become feasible as a new, differential and accurate test of the underlying QCD theory. We present a first step in understanding these shapes and cross sctions in nuclear collisions at the LHC. Our approach allows for detailed simulations of the experimental acceptance/cuts that help isolate jets in the high-multiplicity environment of heavy ion reactions. We demonstrate for the first time that the pattern of stimulated gluon emission can be correlated with a variable quenching of the jet rates and provide an approximately model-independent approach to determine the characteristics of the medium-induced bremsstrahlung spectrum. Surprisingly, in realistic simulations of parton propagation through the QGP we find a negligible increase in the mean jet radius even for large jet attenuation. Jet broadening was found to be manifest in the tails of the angular distributions and its quantification requires high statistics measurements.

PACS numbers:

I. INTRODUCTION

When a fast parton produced by hard scattering propagates in the hot/dense nuclear medium it may suffer multiple scattering with other partons in medium and lose a large amount of energy [1]. This jet quenching mechanism has been used to explain the strong suppressions of hadron spectra at large transverse momenta in nucleus-nucleus collisions observed at RHIC and achieved great successes [2]. To calculate the parton energy loss in nuclear medium several theoretical approaches have been proposed, for example: BDMPS/Zakharov/ASW formalism [3], GLV theory of opacity expansion [4], Higher-twist(HT) approach [5], and AMY formalism [6]. Using different parameters , $\hat{q}$ for BDMPS/Zakharov/ASW , dN_g/dy for GLV , $T_{qg}(x,Q)/f_q(x,Q)$ for HT , and α_s for AMY , these formalisms can describe the striking modifications of hadron spectra in A+A collisions, especially the $R_{AA}(p_T)$ fairly well.

At present, most measurements of hard processes are limited to single particles and particle correlations, which are only the leading fragments of a jet. Though there is general agreement on the physics that controls inclusive particle suppression in the QGP and the experimental methodology of determining $R_{AA}(p_T)$ within $20-25\%$ uncertainty [7] , such measurements have revealed their inherent limitations: the inability to distinguish between phenomenological models of radiative and collisional energy loss, and there exists a staggering order of magnitude uncertainty in the extracted plasma properties via plasma radiography [8]. Experimental interest in multi-particle correlations has stimulated extensive phenomenological work to better constrain the mechanisms of jet-medium interactions [9]. It appears that such modeling effort cannot be systematically improved due to the absence of factorization for the highly differential observables [10]. It is, therefore, critical to find alternatives that accurately reflect the energy flow in strongly-interacting systems, have a more direct connection to the underlying QCD theory, and exhibit a larger discriminating power.

The high rate of hard probes at the LHC and the large-acceptance calorimetry, see e.g. [11], will enable precise jet measurements. Therefore, instead of studying only the leading hadron fragmentated from the jet, we can investigate the modifications of the structure of a jet in hot nuclear medium. To do so one can study jet multiplicity inside a jet cone modified in medium, or the energy flow of the jet in medium [**?**]. Because non-perturbative physics may impose a large impact on jet multiplicity whereas energy flow inside a jet cone can be calculated precisely within the framework of perturbative QCD and needs less non-perturbative input, the latter may provide a more reliable observable to investigate properties of the QGP via jet-medium interactions.

In this paper we will study the jet shape in p+p and heavy-ion collisions, and give the predictions about the jet shape and its R_{AA} in Pb+Pb collisions with $\sqrt{s} = 5500$ GeV at LHC. By varying the radius of the jet cone R_{cone} and the transverse momentum cut ω_{min} we can study the evolution of $R_{AA}(p_T, R_{cone}, \omega_{min})$ for the jet cross section and jet shape to obtain a sequence of curves of $R_{AA}(p_T, R_{cone}, \omega_{min})$ instead of one single line of $R_{AA}(p_T)$ for leading hadron, thus provide an optimistic way to test theoretical models of jet quenching. The central quantity of our discussion is the 'jet shape'. This is a very intuitive quantity - each individual event is probabilistic in nature, but averaged over many events a smooth physical shape can be observed. We consider the jet energy density, as this can be calculated in a partonic framework and carried over hadronization by local parton-hadron duality. This duality exists in phase space, not on individual particles. If we start looking

at the distribution of individual particles, the complications of non-perturbative fragmentation need to be taken into account. But the shape of very high momentum jets should not be significantly affected by non-perturbative processes.

Our discussion of jet shapes in p-p collisions is based on the work by Seymour in [12]. We refer to [12, 13] for discussion of the complications of defining a jet, asking whether a specific particle in the event is part of one jet, another or separate. To make the discussion simpler, we will assume that the complications of the different definitions can be subsumed into an R_{sep} parameter as described below. Once a jet axis and all the jet particles have been found by a jet algorithm, the 'jet shape' is defined as

$$\Psi(r;R) = \frac{\sum_i (E_T)_i \Theta(r - (R_{jet})_i)}{\sum_i \Theta(R - (R_{jet})_i)} \quad (1)$$

where r, R are Lorentz-invariant opening angles, $R_{ij} = \sqrt{(\eta_i - \eta_j)^2 + (\phi_i - \phi_j)^2}$, and i represents a sum over all the particles in this jet. $\Psi(r;R)$ is the fraction of the total jet energy, with a jet having radius R, within radius r. It is automatically normalized so that $\Psi(R;R) = 1$. To move from the integrated to the differential jet shape, we define

$$\psi(r;R) = \frac{d\Psi(r;R)}{dr} \quad (2)$$

This is the angular density of jet energy (remembering that a more visual representation would be $\psi^{vis}(r;R) = \frac{1}{2\pi r}\psi(r;R)$). In terms of a single particle production cross-section, this becomes

$$\psi(r;R) = \frac{\int dE_{T_i} E_{T_i} \frac{d\sigma}{dE_{T_i} dr}}{\int_0^R dr \int dE_{T_i} E_{T_i} \frac{d\sigma}{dE_{T_i} dr}} = \int dz z \frac{d\sigma}{dz dr} \quad (3)$$

where E_{T_i} is the transverse energy of the constituent particles inside the jet cone.

This article will be organized as follows: In Section II, we will outline a calculation of the jet shape in a perturbative framework, compare this calculation to Tevatron data, and extrapolate to LHC energies. A brief discussion of radiative energy loss in GLV formalism, and medium-induced contribution to jet shape due to gluon radiation in medium will be given in Section III. Then in Section IV we will give our numerical calculations of nuclear modification factor for jet cross section and jet shape and discuss their implications. A summary and conclusions will be presented in Section V.

II. JET SHAPES IN 'ELEMENTARY' P-P COLLISIONS

A. Theoretical calculations

1. *leading order results*

In the introduction, we defined the central quantity of our study, the differential jet shape $\psi_a(r;R)$. As in [12], the starting point of the calculation is the leading order parton splitting: a suitable separation of physical time scales enables the separation of the calculation into production and jet showering. The QCD splitting functions $P_{a\to bc}(z)$ give the probability distribution of the large fractional lightcone momenta (or approximately the energy fractions) of the fragments relative to the parent parton, z and $1-z$ respectively. To lowest order, recalling that $\psi_a(r;R)$ describes the energy flow $\propto z$, we can write:

$$\psi_a(r;R) = \frac{d\Psi_a(r;R)}{dr} = \sum_b \frac{\alpha_s}{2\pi}\frac{2}{r}\int_{z_{min}}^{1-Z} dz\, z P_{a\to bc}(z). \quad (4)$$

In Eq. (4) $r = (1-z)\rho$ is related to the opening angle ρ between the final-state partons.

In 'elementary' p+p collisions the inclusion of soft particles ($z_{min} \approx 0$) is not a bad approximation. Even in this case, however, there are intrinsic limitations, related for example to detector acceptance. In heavy ion collisions for the most interesting case of central collisions there is an enormous background of soft particles related to the bulk QGP properties. Jet studies will likely require minimum particle energy $> 1-2$ GeV at RHIC and even more stringent cuts at the LHC. Furthermore, control over z_{min} can provide detailed information about the properties of QGP-induced bremsstrahlung. Further kinematic constraints on the values of z arise since both the resulting partons must be within an angular distance R of the original jet axis, $r < R$, $rz/(1-z) < R$. In this case they are identified with the jet. If not, they are identified as two separate jets. For a cone-based algorithm, the relative separation $R_{sep}R$ (as opposed to just the distance from the original jet axis) is an additional criterion: $\rho < R_{sep}R$. We find:

$$Z = \max\left\{z_{min}, \frac{r}{r+R} \text{ if } r < (R_{sep}-1)R\right\}, \quad (5)$$

$$Z = \max\left\{z_{min}, \frac{r}{R_{sep}R} \text{ if } r > (R_{sep}-1)R\right\}. \quad (6)$$

Carrying out the integration in Eq. (4) we arrive at the

LO jet shape functions for quarks and gluons:

$$\psi_q(r) = \frac{C_F\alpha_s}{2\pi}\frac{2}{r}\left(2\log\frac{1-z_{min}}{Z} - \frac{3}{2}\left[(1-Z)^2 - z_{min}^2\right]\right) , \quad (7)$$

$$\psi_g(r) = \frac{C_A\alpha_s}{2\pi}\frac{2}{r}\left(2\log\frac{1-z_{min}}{Z} - \left(\frac{11}{6} - \frac{Z}{3} + \frac{Z^2}{2}\right)(1-Z)^2 + \left(2z_{min}^2 - \frac{2}{3}z_{min}^3 + \frac{1}{2}z_{min}^4\right)\right) + \frac{T_R N_f\alpha_s}{2\pi}\frac{2}{r}\left(\left(\frac{2}{3} - \frac{2Z}{3} + Z^2\right)(1-Z)^2 - \left(z_{min}^2 - \frac{4}{3}z_{min}^3 + z_{min}^4\right)\right) . \quad (8)$$

In the $z_{min} \to 0$ limit Eqs. (7) and (8) reduce we recover the previously known result [12]. There is an implicit 'plus-prescription' in these results, as we have not considered the virtual corrections in the forward direction. Hence, the result is not applicable for $r = 0$ and does not have the correct normalization when integrated. However, the shape is reflective of final-state parton splitting and For the leading order calculation one may apply a cutoff for small r.

In contrast to the case of $e^+ + e^-$ annihilation, hadronic scattering is accompanied by copious initial-state radiation that can fall within the jet cone. While the contribution of the ISR is small for small values of r/R, it gives an essential contribution at larger angles. A simple estimate based on a dipole radiation and the kinematics of the hard parton - soft gluon coincidence within a cone [?], similar for both quark and gluon jets, yields:

$$\psi_i(r) = \frac{C\alpha_s}{2\pi}2r\left(\frac{1}{Z^2} - \frac{1}{(1-z_{min})^2}\right) \quad (9)$$

Again, the 'plus-prescription' to account for the $r = 0$ point is not explicitly shown. In Eq. (9) $C \simeq C_F \approx C_A/2$.

The leading order calculation is most appropriate for the rare, hard splittings of a very high momentum jet. The use of a running coupling improves this, weighting softer events more and harder events less: we use a running coupling evaluated at the largest k_T in the problem, $r(1-Z)E_T$ for the jet splitting and $(1-Z)E_T$ for the initial state radiation.

2. *Resummation - all orders and multiple emission*

As $r \to 0$, in the collinear limit of parton splitting, the leading order contributions to the jet shape diverge, see Eqs. (7), (8) and (9). In fact, all orders in the perturbative expansion diverge, including powers of $\log r$ in the form $\alpha_s^n \log^{2n-1} r$. With plentiful parton showering, it becomes becomes increasingly less likely that any particular quark and gluon will be coincident with the jet axis. Quantitatively, this is described by a Sudakov form factor. The energy density at small angles is dominated by the hard parton in the splitting. If there is a splitting that leaves the hard parton at an angle r_1, a subsequent splitting at $r_2 < r_1$ will not contribute to the energy density at r_2. Multiple independent splitting follows a Poisson distribution in number, with the P_0 contribution given by e^{-N}. Hence, the probability of emission at an angle less than r is given by the P_0 of emission at angles greater than r, i.e.:

$$P(<r) = \exp(-P_1(>r)) \quad (10)$$

$$= \exp\left(-\int_r^R dr'\,\psi_{Soft}(r')\right) . \quad (11)$$

This only applies for soft emissions which do not take away (much) momentum, i.e. at leading log accuracy. Improvements can be obtained at modified leading log accuracy (MLLA) when the running of the coupling constant is included in P_1. We don't take other (e.g. recoil or kinematic constraints) effects in evaluating the Sudakov form factor in the soft collinear approximation.

The resummed $\psi(r) = \frac{d}{dr}P(<r)$ and we carry out the integration in Eq. (11) including the running $\alpha_S(rE_T)$ to obtain modified leading logarithmic accuracy (MLLA). Note that $\alpha_s(\mu) = 1/(2\beta_0\log\frac{\mu}{\Lambda_{QCD}})$, with $4\pi\beta_0 = b_0 = \frac{11}{3}C_A - \frac{4}{3}T_R N_f$. First, take the small r limit in Eqs. (7), (8) and (9), keeping terms $\propto 1/r$ and $\propto 1/r\log(1/r)$. Based on $Z = \max(z_{min}, r/R)$ in this limit we have two kinematic domains. For $r > z_{min}R$ the results are similar to the known case of no acceptance cut-off and reduces to the known results if $z_{min} = 0$:

$$P_q(r > z_{min}R) = \exp\left(2C_F\log\frac{R}{r}f_1\left(2\beta_0\alpha_s\log\frac{R}{r}\right) - \left[\frac{3}{2}C_F - CR^2 - c_q^{>}(z_{min})\right] \times f_2\left(2\beta_0\alpha_s\log\frac{R}{r}\right)\right) , \quad (12)$$

$$P_g(r > z_{min}R) = \exp\left(2C_A\log\frac{R}{r}f_1\left(2\beta_0\alpha_s\log\frac{R}{r}\right) - \left[\frac{1}{2}b_0 - CR^2 - c_g^{>}(z_{min})\right] \times f_2\left(2\beta_0\alpha_s\log\frac{R}{r}\right)\right) . \quad (13)$$

We find it useful to use the same notation as in [12] and facilitate the comparison to the case of no kinematic cuts: $f_1(x) = \log(1-x)/(2\pi\beta_0)$, and $f_2(x) = (1 - \log(1-x)/x)/(2\pi\beta_0)$. The z_{min}-dependent correc-

tions are isolated as follows:

$$c_q^>(r > z_{min}R; z_{min}) = 2C_F \log(1 - z_{min}) + \frac{3}{2}C_F z_{min}^2 , \quad (14)$$

$$c_g^>(r > z_{min}R; z_{min}) = 2C_A \log(1 - z_{min}) + C_A \left(2z_{min}^2 - \frac{2}{3}z_{min}^3 + \frac{1}{2}z_{min}^4\right) - T_R N_f \left(z_{min}^2 - \frac{4}{3}z_{min}^3 + z_{min}^4\right) . \quad (15)$$

When $r < z_{min}R$ the integration in Eq. (11) has to be split in two regions: $r' \in (r, z_{min}R)$ and $r' \in (z_{min}R, R)$. The second integral is trivially obtained form with $r = z_{min}R$ and combined with the first one yields:

$$P_q(r < z_{min}R) = P_q(r > z_{min}R; r = z_{min}R) \times \exp\left(-\left[\frac{3}{2}C_F - c_q^<(z_{min})\right] \times f_2\left(2\beta_0\tilde{\alpha}_s \log\frac{z_{min}R}{r}\right)\right) , \quad (16)$$

$$P_g(r < z_{min}R) = P_g(r > z_{min}R; r = z_{min}R) \times \exp\left(-\left[\frac{1}{2}b_0 - c_g^>(z_{min})\right] \times f_2\left(2\beta_0\tilde{\alpha}_s \log\frac{z_{min}R}{r}\right)\right) . \quad (17)$$

Here, we denote by $\tilde{\alpha}_s = \alpha_s(z_{min}RE_T)$ as opposed to $\alpha_s = \alpha_s(RE_T)$ and

$$c_q^<(r < z_{min}R; z_{min}) = 2C_F \log\left(\frac{1 - z_{min}}{z_{min}}\right) + 3C_F z_{min} , \quad (18)$$

$$c_g^<(r < z_{min}R; z_{min}) = 2C_A \log\left(\frac{1 - z_{min}}{z_{min}}\right) + C_A \left(4z_{min} - z_{min}^2 + \frac{2}{3}z_{min}^3\right) - T_R N_f \left(2z_{min} - 2z_{min}^2 + 4z_{min}^4\right) . \quad (19)$$

3. *power corrections - an estimate of non-perturbative effects*

We have evaluated the running coupling at the maximum transverse momentum of emitted gluons. If we went one step further and included the running coupling under momentum transfer integrals, then we would have contributions from regions in which $Q \sim \Lambda_{QCD}$ or lower, i.e. there is a fundamental non-perturbative contribution to all of the integrals. An estimate of these power correction effects with finite acceptance is as follows:

$$\psi_{PC}(r) = \frac{2C_R}{2\pi}\frac{2}{r}\frac{Q_0}{rE_T}\left(\bar{\alpha_0}'(Q_0, k_{min}) - \alpha_s(\mu) - 2\beta_0\alpha_s(\mu)^2\left(1 + \log\frac{\mu}{Q_0}\right)\right) + \frac{2C_R}{2\pi}\frac{2}{r}\frac{k_{min}}{rE_T}\left(\alpha_s(\mu) + 2\beta_0\alpha_s(\mu)^2\left(1 + \log\frac{\mu}{k_{min}}\right)\right) , \quad (20)$$

where $C_R = C_F, C_A$ for quarks, gluons respectively, $k_{min} = z_{min}rE_T$, μ is the renormalization scale. The first term in the first parentheses $\bar{\alpha_0}'(Q_0, k_{min})$ is the parametrized non-perturbative contribution and defined as:

$$\bar{\alpha_0}'(Q_0, k_{min}) = \frac{1}{Q_0}\int_{k_{min}}^{Q_0} dk\alpha_s(k) . \quad (21)$$

In our numerical calculation we use

$$\bar{\alpha_0}'(2GeV, 0) = 0.52 , \ \bar{\alpha_0}'(3GeV, 0) = 0.42$$

from ref.[12, 14] and the parametrization of strong coupling constant at small momentum transfer in ref.[15]. The second and the third terms in the first parentheses come from subtracting off the perturbative component in the non-perturbative region[14], while the term in the second parentheses results from the introduction of detector acceptance z_{min}.

A similar expression is used for the initial state radiation:

$$\psi_{i,PC}(r) = \frac{2C_R}{2\pi}2r\frac{Q_0}{E_T}\left(\bar{\alpha_0}'(Q_0, k_{min}) - \alpha_s(\mu) - 2\beta_0\alpha_s(\mu)^2\left(1 + \log\frac{\mu}{Q_0}\right)\right) + \frac{2C_R}{2\pi}2r\frac{k_{min}}{E_T}\left(\alpha_s(\mu) + 2\beta_0\alpha_s(\mu)^2\left(1 + \log\frac{\mu}{k_{min}}\right)\right) , \quad (22)$$

The power corrections are in fact sizeable for lower jet energies, even at large r. This suggests that any deviation of these results from experimental results may be due to incomplete consideration of non-perturbative effects. Note that the generalization of power corrections to finite acceptance implies that these should be taken into account only for $z_{min}rE_T < Q_0$.

4. *Total contribution to the jet shape*

As mentioned before the resummed jet shape at small r/R is evaluated as $\psi_{resum}(r) = \frac{d}{dr}P(r) = \psi_{coll}(r)P(r)$.

Taking all contributions to the jet shape and ensuring that there is no double counting at small r/R to $\mathcal{O}(\alpha_f^{\in})$ we find:

$$\psi(r) = \psi_{coll}(r)\,(P(r)-1) + \psi_{LO}(r) + \psi_{LO,i}(r) + \psi_{PC}(r) + \psi_{i,PC}(r)\,, \quad (23)$$

where on right-hand-side of the equation the first term comes from Sudakov resummation with subtraction off their leading order contribution at small r/R, the second and third terms give the leading-order contributions in the final-state and the initial-state, the fourth and fifth terms represent contributions from power correction in the final-state and the initial-state.

Our normalization will now be off - in any comparison with experimental data the difference between the integral of $\psi(r)$ and 1 is taken off the most inner bin.

B. Comparison to Tevatron data

This simple calculation gives a decent interpretation of high p_T jet shape data. The R_{sep} is often taken as a free parameter and fixed by comparison with data [13]. R_{sep} is usually jet momentum dependent and it is found that at high jet momentum usually theoretical calculations with $R_{sep} = 1.3$ can give a good fit to experimental data [13]. But at lower jet momentum to fit the data we usually need a larger R_{sep} [16].

In Fig. 1 we show the comparison of the numerical results of jet shape with our theoretical model described above calculations with the experimental measurements of jet shape in $p\bar{p}$ collisions at $\sqrt{s} = 1960$ GeV at Fermilab in Run II (CDF II) [17]. In numerical calculations we include all contributions from leading order, resummation and power corrections and compare to data by varying the parameter R_{sep}. From Fig. 1 we can see that at high jet momentum our theoretical model give very good descriptions on experimental data at CDF II with $R_{sep} = 1.3 - 1.4$. At low jet momentum to fit the data larger R_{sep} may be needed at with jet momentum $E_T = 45 - 55$ GeV, we find that our model with $R_{sep} = 2$ can describe the data fairly well except at very small r/R region. The derivation of theoretical calculations from experimental data in small r/R region at low jet momentum may be due to large non-perturbative effects. In the insert of Fig. 1 we give the values of R_{sep} at different jet momenta used in our numerical calculations.

By comparing numerical calculations of our theoretical model with experimental measurements as illustrated in Fig. 1, we can see the our simple model is not sufficient to give a good description of the lower momentum data at Tevatron, without resorting to a momentum dependent R_{sep} parameter. This may be due to a change in momentum dependence at NLO the breakdown of our soft collinear jet splitting approximations. In other studies with Monte-Carlo event generators, tweaking of the initial state radiation (from multiple parton interactions)

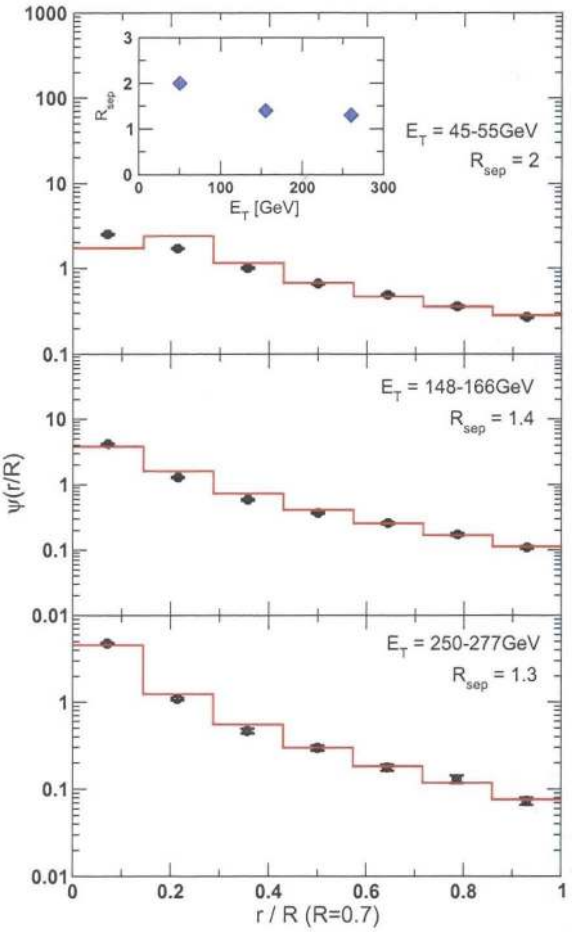

FIG. 1: Comparison of numerical results of our theoretical mode with experimental data of jet shape with $\sqrt{s} = 1960$ GeV by CDF.

was seen to be important - a more advanced treatment of this aspect may improve the result. More fundamentally, the deficiencies at lower momenta may be due to non-perturbative effects (as evidenced by the small change by including a rough estimate of the power corrections) or finite time effects and interference with the production diagrams.

Nevertheless, by varying R_{sep} our numerical results of theoretical computations agree quite well with the data at CDF II. The fitting values of R_{sep} at different jet momenta to CDF data will then be fixed and used in our later numerical calculations of jet shape in vacuum and in medium at LHC with center of mass energy $\sqrt{s} = 5500$ GeV.

C. Predictions for the LHC

We use our theoretical model for CDF and apply the same momentum dependent R_{sep} parameter to predictions for the LHC. The emphasis here is not on the best

possible prediction for the jet shapes in p-p collisions at the LHC, but the derivation of a simple model for the baseline comparison when doing calculations for Pb-Pb collisions. The only difference we make between CDF and the LHC is in production: we should take a different ratio of gluon to quark jets. As we're moving to a higher collision energy, the collisions at LHC will have a greater gluon contribution than for the lower CDF energies, which can be seen clearly in the insert of Fig. 12 in Appendix. Therefore the LHC result is expected to be slightly wider than the CDF result.

In Fig. 3 we demonstrate our numerical results of jet shape at different jet energies with two jet cone radii $R = 0.7$ and $R = 0.4$ in p+p collisions with $\sqrt{s} = 5500$ GeV at LHC. From jet energy $E_T = 50$ GeV to jet energy $E_T = 500$ GeV, one can see jet shape becomes steeper, which implies that with higher jet energy, the forward radiation will be more favored. By increasing cone radius from $R = 0.4$ to $R = 0.7$, jet shape will be wider due to more energy carried away by soft radiation will be found inside a larger cone radius. On the other hand, by imposing an acceptance cut $\omega_{min} = 10$ GeV, jet shape will be shifted to smaller r/R region with higher peak because the forward radiation becomes more pronounced by cutting the contribution of soft radiation. However, the differences of jet shapes due to different choices of jet cone radius R and acceptance cut ω_{min} may die out with increasing jet energy E_T as shown in Fig. 3. This observation could be explained by the fact that at very high jet energy, jet shape has been very steep already because of dominated forward radiation, and there are fewer contributions from hard or large-angle radiations. By varying cone radius and acceptance cut, the contribution from hard or large-angle radiations will be changed a little accordingly, but not significantly, and hence affect jet shape at very high jet energy slightly.

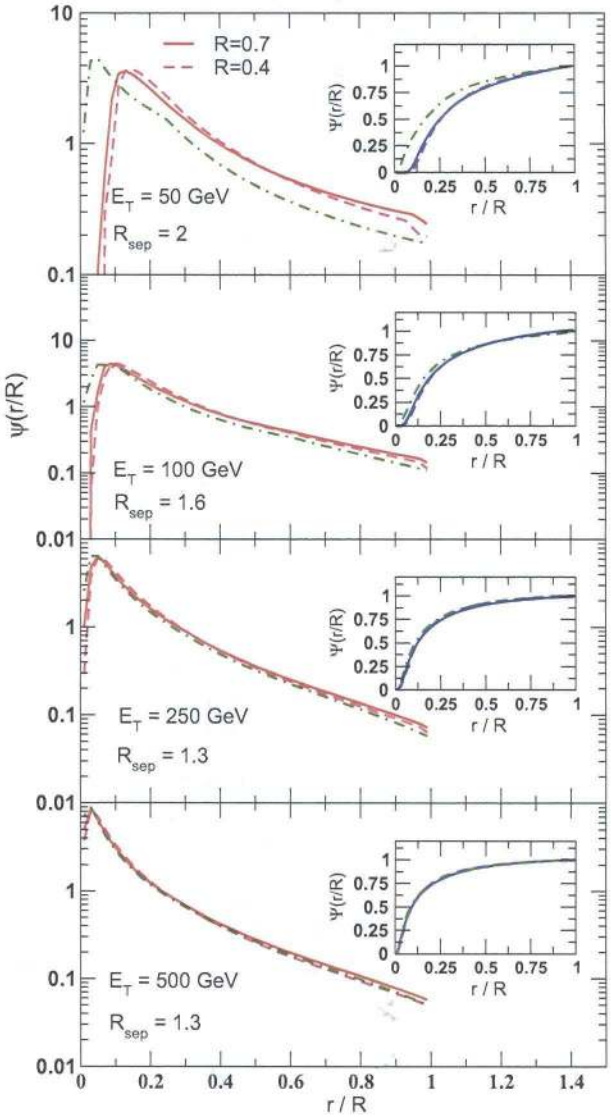

FIG. 2: (Color online) Numerical predictions for jet shape at p+p collisions with $\sqrt{s} = 5500$ GeV at LHC. Solid line represents jet shape with $R = 0.7$, $\omega_{min} = 0$ GeV, dash line stands for jet shape with $R = 0.4$, $\omega_{min} = 0$ GeV, and dash-dot line is for jet shape with $R = 0.7$, $\omega_{min} = 10$ GeV. The insert shows the integrated jet shapes.

III. MEDIUM-INDUCED CONTRIBUTION TO THE JET SHAPE

The principal medium-induced contribution to a jet shape comes from the radiation pattern of the fast quark or gluon, stimulated by their propagation and interaction in the QGP. There is a simple heuristic argument which allows one to understand how interference and coherence effects in QCD amplify the difference between the energy distribution in a vacuum jet and the in-medium jet shape [26]. Any destructive effect on the integral average parton energy loss ΔE^{rad}, such as the Landau-Pometranchuk-Migdal effect, can be traced at a differential level to the attenuation or full cancellation of the collinear, $k_T \ll \omega$, gluon bremsstrahlung:

$$\Delta E^{rad}_{\text{LPM suppressed}} \Rightarrow \frac{dI^g}{d\omega}(\omega \sim E)_{\text{LPM suppressed}} \Rightarrow \frac{dI^g}{d\omega d^2k_T}(k_T \ll \omega)_{\text{LPM suppressed}}\,, \tag{24}$$

and we indicate the parts of phase space where the modification of the incoherent $dI^g/d\omega d^2k_T$ is most effective.

Indeed, detailed derivation of the coherent inelastic parton scattering regimes in QCD was given in [23]. In all cases, the origin of the LPM suppression can be traced to the cancellation of the collinear bremsstrahlung. The destructive quantum interference is most prominent for final-state radiation, where the large-angle gluon bremsstrahlung was originally discussed in [25] to first order in opacity. Even though to carry out realistic simulations to higher orders in opacity with full geometry will require computational power beyond what is cur-

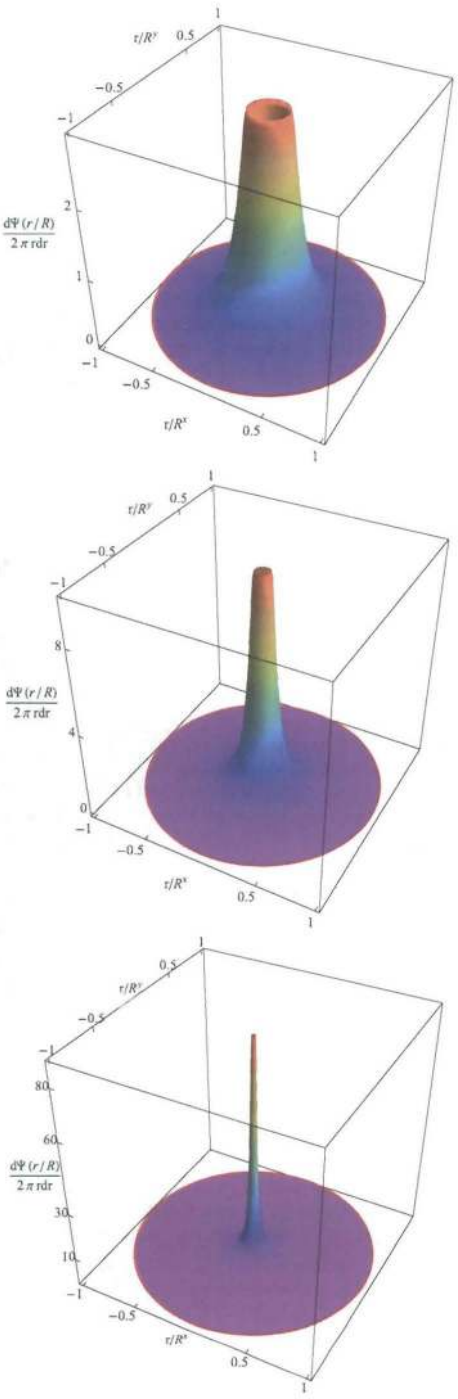

FIG. 3: (Color online) Numerical predictions for jet shape at p+p collisions with $\sqrt{s} = 5500$ GeV at LHC. Solid line represents jet shape with $R = 0.7$, $\omega_{min} = 0$ GeV, dash line stands for jet shape with $R = 0.4$, $\omega_{min} = 0$ GeV, and dash-dot line is for jet shape with $R = 0.7$, $\omega_{min} = 10$ GeV. The insert shows the integrated jet shapes.

rently available, we first present an analytic proof that a cone-like pattern of medium-induced emission persists to all orders in the correlations between multiple scattering centers (elementary emitters) and we focus on the case of immediate interest: light quark and gluon jets and final-state bremsstrahlung. Generalization to massive partons can easily be achieved, see e.g. [24], but it is important to note that the effect of a heavy quark mass versus the jet energy depends on the coherent scattering regime [23].

A. Radiative energy loss in the GLV formalism

In our calculation we will use GLV formalism of expanding the medium-induced radiation in the correlations between multiple scattering centers [23]. We first recall the definitions of the Hard, Gunion-Bertsch and Cascade propagators in terms of the gluon transverse momentum $\mathbf{k}$ and the transverse momentum transfers from the medium $\mathbf{q}_i$:

$$\begin{aligned} \mathbf{H} &= \frac{\mathbf{k}}{\mathbf{k}^2}\,, \mathbf{C}_{(i_1 i_2 \cdots i_m)} = \frac{(\mathbf{k} - \mathbf{q}_{i_1} - \mathbf{q}_{i_2} - \cdots - \mathbf{q}_{i_m})}{(\mathbf{k} - \mathbf{q}_{i_1} - \mathbf{q}_{i_2} - \cdots - \mathbf{q}_{i_m})^2}\,, \\ \mathbf{B}_i &= \mathbf{H} - \mathbf{C}_i\,, \mathbf{B}_{(i_1 \cdots i_m)(j_1 \cdots i_n)} = \mathbf{C}_{(i_1 \cdots j_m)} - \mathbf{C}_{(j_1 \cdots j_n)}\,, \end{aligned} \tag{25}$$

The relevant inverse gluon formation times can be written as:

$$[\tau^f_{(i_1 i_2 \cdots i_m)}]^{-1} = \omega_{(i_1 i_2 \cdots i_m)} = [k^+ |\mathbf{C}_{(i_1 i_2 \cdots i_m)}|^2]^{-1}\,. \tag{26}$$

For final-state radiation, the intensity spectrum reads:

$$k^+\frac{dN^g(FS)}{dk^+d^2\mathbf{k}} = \frac{C_R\alpha_s}{\pi^2}\sum_{n=1}^{\infty}\left[\prod_{i=1}^{n}\int\frac{d\Delta z_i}{\lambda_g(z_i)}\right]\left[\prod_{j=1}^{n}\int d^2\mathbf{q}_j\left(\frac{1}{\sigma_{el}(z_j)}\frac{d\sigma_{el}(z_j)}{d^2\mathbf{q}_j}-\delta^2(\mathbf{q}_j)\right)\right]$$
$$\times\left[-2\,\mathbf{C}_{(1,\cdots,n)}\cdot\sum_{m=1}^{n}\mathbf{B}_{(m+1,\cdots,n)(m,\cdots,n)}\left(\cos\left(\sum_{k=2}^{m}\omega_{(k,\cdots,n)}\Delta z_k\right)-\cos\left(\sum_{k=1}^{m}\omega_{(k,\cdots,n)}\Delta z_k\right)\right)\right], \quad (27)$$

where $\sum_2^1 \equiv 0$ and $\mathbf{B}_{(n+1,n)} \equiv \mathbf{B}_n$ is understood. In the case of final-state interactions, $z_0 \approx 0$ is the point of the initial hard scatter and $z_L = L$ is the extent of the medium. The path ordering of the interaction points, $z_L > z_{j+1} > z_j > z_0$, leads to the constraint $\sum_{i=1}^{n}\Delta z_i \leq z_L$. One implementation of this condition would be $\Delta z_i \in [\,0, z_L - \sum_{j=1}^{i-1}\Delta z_j\,]$ and it is implicit in Eq. (27).

There is an obvious limit of the GLV radiative spectrum when $L \gg \lambda_g \gg \tau_f$, where λ_g is the mean free path of the gluon in hot QGP. Here, the contributions of cos terms vanish after integration over the unobserved $\mathbf{q}_i$ or Δz_i due to rapid oscillation. It is easy to see in this limit for n=1 that,

$$k^+\frac{dN^g}{dk^+} = \frac{C_R\alpha_s}{\pi^2}\left\langle\frac{L}{\lambda_g}\right\rangle\int d^2\mathbf{k}\int d^2\mathbf{q}_1 \times\left\langle\frac{1}{\sigma_{el}}\frac{d\sigma_{el}}{d^2\mathbf{q}_1}\right\rangle\left[\mathbf{C}_1^2-\mathbf{H}^2+\mathbf{B}_1^2\right]. \quad (28)$$

In the very high energy limit $E \to \infty$, leading to a large $\mathbf{k}$ phase space, a change of variables $\mathbf{k} \to \mathbf{k} - \mathbf{q}_1$ shows that the first two terms in Eq. (28), cancel, leading to an incoherent Bertsch-Gunion gluon emission in a hot QGP medium with $\langle n\rangle = \frac{L}{\lambda_g}$. By direct inspection one can see that $n > 2$ terms do not contribute. In fact, it is easy to verify that for any bremsstrahlung regime, initial-state, final-state and no hard scattering, this limit holds [23]. More generally, in this limit it can be shown that the Reaction Operator $\hat{R} \to 0$. Naturally, for finite jet energies there will be corrections when $k^+dN^g/dk^+d^2\mathbf{k}$ is evaluated numerically with actual kinematic bounds.

B. Collinear radiation in GLV formalism

The example given above illustrates that while limits can be imposed and taken in the GLV results, such limits are artificial in that the formation time of the gluon at the emission vertex spans $\tau_f \in (0,\infty)$. The Reaction Operator approach is not an approach of averages but compares differentially τ_f to the separation between the scattering centers. For example, even when $\mathbf{k} \to 0$ the formation time can be small or large, depending on the momentum transfers for the medium. Let us investigate this case in more detail: we note that $k^+ \approx 2\omega$ and $\mathbf{k} \approx r\omega\hat{n}$, where r is the angle relative to the jet axis. Here, $\hat{n}$ is a unit vector transverse to the jet axis which defines the azimuthal angle ϕ of gluon emission. Using the results of Eq. (27), the 2D (ϕ, r) angular distribution of gluons at n-th order in the correlated scattering expansion reads:

$$\lim_{r\to 0}\frac{\omega dN^g}{d\omega d\phi dr} \propto \omega\left[\prod_{j=1}^{n}\int d^2\mathbf{q}_j\left(\frac{1}{\sigma_{el}(z_j)}\frac{d\sigma_{el}(z_j)}{d^2\mathbf{q}_j}-\delta^2(\mathbf{q}_j)\right)\right]\frac{\mathbf{q}_1+\cdots+\mathbf{q}_n}{(\mathbf{q}_1+\cdots+\mathbf{q}_n)^2}\cdot\sum_{m=1}^{n}\omega r\left(\frac{\mathbf{q}_{m+1}+\cdots+\mathbf{q}_n}{(\mathbf{q}_{m+1}+\cdots+\mathbf{q}_n)^2}\right.$$
$$\left.-\frac{\mathbf{q}_m+\cdots+\mathbf{q}_n}{(\mathbf{q}_m+\cdots+\mathbf{q}_n)^2}\right)\times\left(\cos\left(\sum_{k=2}^{m}\frac{(\mathbf{q}_k+\cdots+\mathbf{q}_n)^2}{2\omega}\Delta z_k\right)-\cos\left(\sum_{k=1}^{m}\frac{(\mathbf{q}_k+\cdots+\mathbf{q}_n)^2}{2\omega}\Delta z_k\right)\right). \quad (29)$$

Here, we have already set $r = 0$ where possible. To use this general notation we have to clarify certain special cases: for $m = n$ we have $\cos[(\mathbf{q}_{n+1}+\mathbf{q}_n)^2\Delta z_{n+1}/2\omega] \equiv 1$. For the transverse propagators and m we have $\omega r(\mathbf{q}_{n+1}+\mathbf{q}_n)/(\mathbf{q}_{n+1}+\mathbf{q}_n)^2 \equiv \hat{n}$. It is know that the leading $n = 1$ contribution to final-state medium-induced radiation leads to $\lim_{r\to 0}\omega dN^g/d\omega d\phi dr = 0$ [25]. Our goal is to show that this result is general and holds to any order in the expansion. Its implications are that there is very little overlap between the techniques used to compute the "vacuum" and medium-induced contributions to the jet shape. A general proof requires demonstration of the absence of unprotected divergences for any set of momentum transfers $\{\mathbf{q}_i\}$, finiteness of the momentum transfer integrals as $\mathbf{q}_i \to \infty$ and a mechanism that kills the small-angle contribution.

1. We now look at the the large $\mathbf{q}_i$ limit. The transverse propagator contribution itself in Eq. (29) be-

haves as $\sim 1/\mathbf{q}_i^2$. Furthermore, irrespective of the small $\mathbf{q}_i$ behavior of the momentum transfer distribution from the medium, for large momentum transfers the cross section is suppressed by the Rutherford $\sim 1/\mathbf{q}_i^4$ behavior, ensuring the finiteness of the integrals.

2. Next, we examine the potential singularity as $|\mathbf{q}_1 + \cdots + \mathbf{q}_n| \to 0$. The difference in the LPM interference terms in this limit goes as $\mathcal{O}((\mathbf{q}_1 + \cdots + \mathbf{q}_n)^2)$ and for the most problematic transverse propagator term even as $\mathcal{O}((\mathbf{q}_1 + \cdots + \mathbf{q}_n)^4)$. In summary, not only is there no divergence, but the integrand vanishes.

3. We now collect the interference phases associated with problematic propagators as $|\mathbf{q}_k + \cdots + \mathbf{q}_n| \to 0$, $1 < k \leq n$. Expanding around a small net transverse momentum sums we find that the singularity is canceled:

$$\left[\sin\sum_{j=2}^{k-1}\frac{(\mathbf{q}_j+\cdots+\mathbf{q}_n)^2}{2\omega}\Delta z_j - \sin\sum_{j=1}^{k-1}\frac{(\mathbf{q}_j+\cdots+\mathbf{q}_n)^2}{2\omega}\Delta z_j\right]\frac{(\mathbf{q}_k+\cdots+\mathbf{q}_n)^2}{2\omega}\Delta z_k \,. \tag{30}$$

Actually, the lack of singularities persists also away from the small r limit.

4. With the integrand well behaved and all integrals finite we see that the phase space factor r in the numerator is sufficient to ensure vanishing medium-induced bremsstrahlung contribution at the center of the jet. It is assisted by partial cancellation from angular integrals of the type $\int \mathbf{q}_i \cdot \mathbf{q}_j f(\mathbf{q}_i, \mathbf{q}_j) d\phi_{ij}$. It is only for the special case of $\hat{n} \cdot (\mathbf{q}_1 + \cdots + \mathbf{q}_n)$ where the antisymmetric integrand under $\mathbf{q}_i \to -\mathbf{q}_i$ for all i fully ensures the vanishing zero-angle radiative contribution.

This completes our proof that at any order in opacity

$$\lim_{r\to 0}\frac{\omega dN^g_{\rm med}}{d\omega d\phi dr} = 0 \,. \tag{31}$$

Numerical simulations, using Monte-Carlo techniques, confirm independently that $dI^g/d\omega d^2\mathbf{k}$ vanishes as $\mathbf{k} \to 0$ [30?].

C. Numerical methods and QGP properties

Results relevant to the LHC phenomenology are calculated using full numerical evaluation of the medium-induced contribution to the observed jet shapes and the modification of the in-medium cross sections. Jet production, being rare in that $\sigma(E_T > E_{T\ \rm min})T_{AA}(b) \ll 1$, follows binary collision scaling $\sim d^2N_{\rm bin.}/d^2\mathbf{x}_\perp$. In contrast, the medium is distributed according to the number of participants density $\sim d^2N_{\rm part.}/d^2\mathbf{x}_\perp$. Soft particles that carry practically all of the energy that is stopped in a heavy ion collision cannot deviate a lot from such scaling. We take into account longitudinal Bjorken expansion since transverse expansion leads to noticeable corrections only in the extreme $\beta_T \to 1$ limit [28]. In our approach all relevant finite time and finite kinematics integrals, such as the ones over the separation between the scattering centers $\Delta z_i = z_i - z_{i-1}$, the bremsstrahlung gluon phase space $\Lambda_{QCD} < \omega < E_{\rm jet.}$, $\Lambda_{QCD} < k_\perp < 2\omega$ [33], and the transverse momentum transfers $0 < q_i < \sqrt{s/4} = \sqrt{m_D E_{\rm jet}/2}$, are done numerically [23]. In our simulation we generated in-plane jets, $\phi_{\rm jet} - \phi_{\rm reaction\ plane} = 0$. This is of little importance in central Pb+Pb collisions (b=3 fm), where the medium effects on jet propagation are most pronounced, but in semi-central (b=8 fm) and peripheral (b=13 fm) reactions this will lead to smaller than average energy loss.

The evolving intrinsic momentum and length scales in the QGP expected to be created at the LHC are determined as follows: we first estimate the QGP formation time $\tau_0 = 1/\langle p_T\rangle = 0.23$ fm, where $\langle p_T\rangle \approx 850$ MeV was obtained from extrapolations to LHC energies made by using Monte Carlo event generator results, fit to the CDF collaboration data from $\sqrt{s} = 1.8$ GeV $p + \bar{p}$ collisions [31]. Here we account for the observed $\sim 25\%$ increase in the mean transverse momenta in going from $N + N$ to $A + A$ collisions at RHIC. Gluons dominate the soft parton multiplicities at the LHC and their time- and position- dependent density can be related to charged hadron rapidity density in the Bjorken expansion model [32]:

$$\rho = \frac{1}{\tau}\frac{d^2(dN^g/dy)}{d^2\mathbf{x}_\perp} \approx \frac{1}{\tau A_\perp}\frac{3}{2}\left|\frac{d\eta}{dy}\right|\frac{d^2(dN^{ch}/d\eta)}{d^2\mathbf{x}_\perp} \,. \tag{32}$$

Here, $dN^{ch}/d\eta = \kappa N_{\rm part.}/2$ with $\kappa \approx 9$ for $\sqrt{s} = 5.5$ TeV. The following table summarizes characteristics of Pb+Pb collisions at the LHC and initial QGP properties. An inelastic cross section $\sigma_{in} = 65$ mb has been used in an optical Glauber model where necessary. Note that in Table [?] the quoted mean temperatures, Debye screening scales and gluon mean free paths are obtained as averages

Class	Central	Mid-central	Peripheral
$b\ [fm]$	3	8	13
N_{part}	361	165	18
dN^g/dy	2800	1278	137
$\langle T(\tau_0)\rangle$ [MeV]	751	693	426
$\langle m_D(\tau_0)\rangle$ [GeV]	1.89	1.73	1.07
$\langle \lambda_g(\tau_0)\rangle$ [fm]	0.25	0.27	0.46

TABLE I: Summary of the relevant energy loss parameters for central, semi-central and peripheral collisions at $\sqrt{s} =$ 5.5 TeV collisions at the LHC.

with the binary collisions weight $T_{AA}(\mathbf{x}_\perp; b)$. In our evaluation we use $g_s = 2.5$, $(\alpha_s = 0.5)$ to describe the scattering of the jet with the medium but the QGP-induced bremsstrahlung is calculated with a running $\alpha_s(k_\perp)$ for emission vertex, similar to the MLLA approach for the vacuum jet shapes.

Assuming local thermal equilibrium one finds:

$$T(\tau, \mathbf{x}_\perp) = \sqrt[3]{\pi^2 \rho(\tau, \mathbf{x}_\perp)/16\zeta(3)}\,, \tau > \tau_0\,. \qquad (33)$$

The Debye screening scale is given by $m_D = gT$, recall that we work in the approximation of a gluon-dominated plasma and $N_f = 0$. The relevant gluon mean free path is easily evaluated: $\lambda_g = 1/\sigma^{gg}\rho$ with $\sigma^{gg} = (9/2)\pi\alpha_s^2/m_D^2$

Evaluation of the medium-induced energy loss and its contribution to jet shapes is numerically expensive. Exact results have been obtained only for $E_{\rm jet} = 20$, 100 and 500 GeV. We interpolate for other values of interest.

D. Energy loss distribution

A consistent energy loss theory provides complete information for the differential distribution of the lost ΔE_{rad}, i.e. the bremsstrahlung spectrum in Eq. (27). The main point that we want to make here is that the this distribution is completely determined by the poroperties of the QGP and the mechanisms of energetic quark and gluon stopping in hot and dense matter. Therefore, selecting different jet radii R and $p_{T\ \rm min}$ of the particles will significantly alter both the jet shape and the ammount of energy lost by the hard parton which can be recovered in the experimental measurement. In contrast, we have seen in Fig. 3 that the jet shapes scale approximately as a funcion of r/R, i.e. they are independent of the selection of cone opening angle R. The jet cross section weakly depends on R, unless $R \to 0$. Finally, $z_{min} = 0.1 - 0.2$ is necessary to noticeably alter the jet shape, implying that $\sim 20\%$ of the parent partoin enegy has to be missed via $p_{T\ \rm min}$ cuts to observe significant effects on $\psi_{vac}(r)$.

A clear experimental strategy will then be to use the leverage arm provided by $R\ (= R^{max}$ in the evaluation of the $\Delta E_{\rm rad})$ and $p_{T;\rm min}\ (= \omega^{min}$ in the evaluation of the $\Delta E_{\rm rad})$ to determine the distribution of the lost energy. This is illustrated schematically in Fig. 4. Theoretically, the first quantity to be calculated theoretically is:

$$\frac{\Delta E^{in}}{E}(R^{\rm max}, \omega^{\rm min}) = \frac{1}{E}\int_{\omega^{\rm min}}^{E}\int_0^{R^{\rm max}} \frac{dI^g}{d\omega dr}(\omega, r)\,. \qquad (34)$$

We present in a 3D Fig. 5 this fractional energy loss for a quark jet and a gluon jet with energy $E_{jet} = 20$ GeV inside the jet cone to the as a function of jet radius $R_{\rm max}$ and the acceptance cut $\omega^{\rm min}$. Increasing R_{max} or decreasing the acceptance cut $\omega^{\rm min}$ we will recover more of the paent parton energy, lost via gluon bremsstrahlung. We note that in Fig. 5 the mean energy loss was calculated as an average over the probability distribution

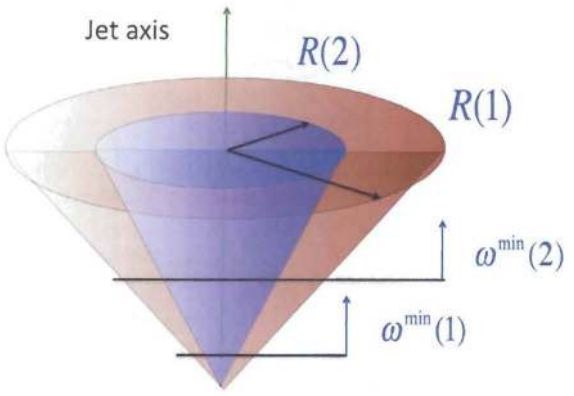

FIG. 4: (Color online) Schematic illustration of the cone radius selection R and the and the particle/tower p_T / E_T. The measured energy is the one that falls above ω_{min} and within R.

$P(\epsilon; E)$ [?], reflective of multi-gluon fluctuations:

$$\langle\epsilon\rangle = \langle\frac{\Delta E}{E}\rangle = \int_0^1 d\epsilon\ \epsilon P(\epsilon; E)\,. \qquad (35)$$

For large fractional energy loses, such as the illustrative example of a 20 GeV jet in central $Pb + Pb$ collisions at the LHC, $\Delta E_g/\Delta E_q$ is much smaller than the asymptotic ratio $C_A/C_F = 9/4$ due to the kinematic constraint $\Delta E < E$ [18].

The separate dependences of $\Delta E^{in}(R^{\rm max}, \omega^{\rm min})/E$ on the cone radius an the momentum acceptance cut are more clearly illustrated in Fig. 6. We show central, mid-central and peripheral collisions, impact paramters $b = 3,\ 8,\ 13$ fm, respectively, in Pb+Pb collisions at LHC with $\sqrt{s} = 5500$ GeV. We notice that the ratio $\Delta E^{in}/E(R^{max}, \omega^{min})$ goes down at larger impact parameters because the energy loss of the jet decreases in peripheral collisions. However, at each impact parameter there is a variation of the amount of the bremsstrahlung energy, recovered in the cone. This is precisely the variation that will map on a variable $R_{AA}^{jet}(R^{max}, \omega^{min})$. For example, in the limit of a very small opening angle and/or large momentum cut to eliminate the softer QGP-induced radiation the suppression should approximate that of leading hadrons (up to differences arising form the possibly softer particle spectra due to fragmentation).

$$R_{AA}^{jet}(R^{max} \to 0 \text{ and/or } \omega^{min} \to E) = R_{AA}^{\text{leading parton}} \approx R_{AA}^{h^\pm}\,. \qquad (36)$$

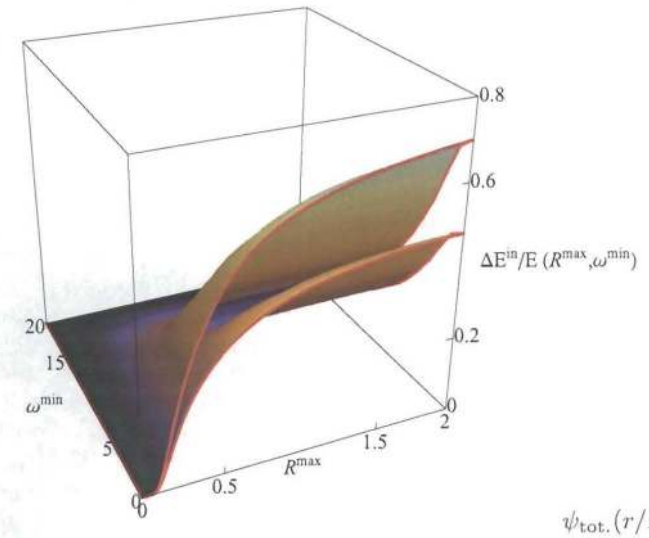

FIG. 5: (Color online) 3-D plot for the ratio of the energy partons lose inside a jet cone of opening angle $R^{\max}$ with $\omega > \omega^{\min}$ to the total parton energy. We have chosen a jet of energy $E_{jet} = 20$ GeV in b=3 fm Pb+Pb collisions at LHC and varied the jet radius R^{max} and the acceptance cut ω^{min}. The upper surface is for a gluon jet and the lower surface is for a quark jet.

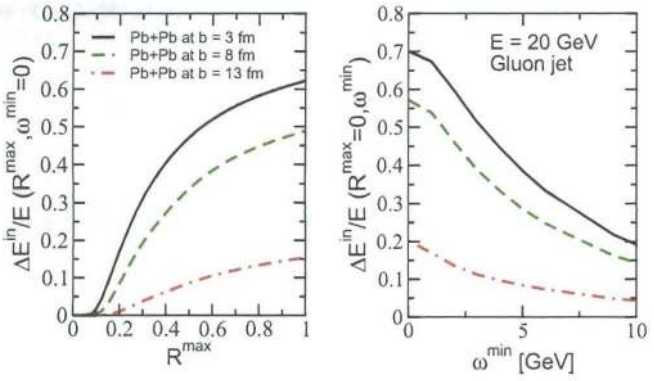

FIG. 6: (Color online) 1D projections of Eq. (34) The left panel shows the trend vs the jet radius R^{max} ($\omega^{\min} = 0$) and the right panel shows the trend versus the acceptance cut ω^{min} ($R^{max} = R^{\infty}$). A gluon jet of $E_{jet} = 20$ GeV in $b =$ 3, 8, ; 13 fm Pb+Pb collisions at LHC was used as an example

IV. THE SHAPE OF JETS IN HEAVY ION COLLISIONS

The ability to select the cone radius R and the minimum particle energy $p_{T\ \min}$ will allow for the first time for a full 2D reconstruction of QGP-induced bremsstrahlung spectrum both in angle $r \approx k_T/\omega$ and energy ω. This approach relies on the fact that the shape functions $\psi_{\rm vac.}(r/R)$ and $\psi_{\rm med.}(r/R) = (1/\Delta E_{rad})dI^g/dr$ are substantially different. The full medium-modified jet shape can be calculated basing on the formulas as:

$$\frac{\sigma^{AA}(R,\omega^{min})}{d^2E_T dy} = \int_{\epsilon=0}^{1} P(\epsilon; R, \omega^{min}) \times \left(\frac{1}{(1-(1-f(R/\infty;\omega/0))\epsilon)^2} \frac{\sigma^{pp}(R,\omega^{min})}{d^2E'_T dy} \right), \tag{37}$$

where $E'_T = E_T/(1-(1-f)\epsilon)$, $f(R/\infty, \omega^{min}/0)$ is the fraction of the lost energy that falls within the jet cone R and carried by gluons of $\omega > \omega_{min}$ defined by:

$$f(R/\infty, \omega^{min}/0) = \frac{\Delta E((0,R),(\omega,\infty))}{\Delta E((0,\infty),(0,\infty))}\,. \tag{38}$$

The full medium-modified jet shape is given by:

$$\psi_{\rm tot.}(r/R) = \frac{1}{\rm Norm}\int_0^1 d\epsilon\, P(\epsilon, R, \omega_{min}) \left(\frac{1}{(1-\epsilon)^2} \frac{d\sigma^{\rm pp}(R, p_{T\ \rm min})}{d^2E'_T dy} \psi_{\rm vac.}(r/R) + \frac{1}{(f(R/\infty, p_{T\ \rm min}/\infty)\epsilon)^2} \frac{d\sigma^{\rm pp}(R, p_{T\ \rm min})}{d^2E''_T dy} \psi_{\rm med.}(r/R) \right) ($$

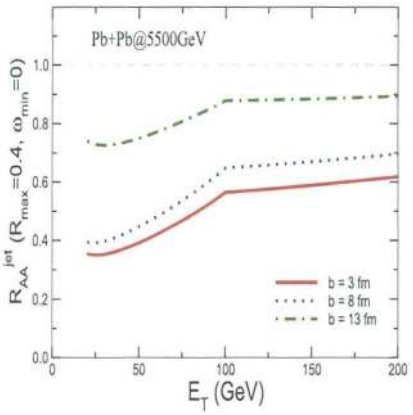

FIG. 7: (Color online) Nuclear modification factor $R_{AA}^{jet}(R_{max}, \omega_{min})$ as a function of jet energy E_T at impact parameters $b = 3$ fm (solid line), $b = 8$ fm (dot line) and $b = 13$ fm (dash-dot line) in Pb+Pb collisions with $\sqrt{s} = 5500$ GeV.

With the numerical methods and relevant parameters described in last Section we can calculate numerically nuclear modification factor $R_{AA}^{jet}(R_{max}, \omega_{min})$ and jet shape in Pb+Pb collisions at central of mass energy $\sqrt{s} = 5500$ GeV. Fig. 7 illustrates jet energy E_T dependent $R_{AA}^{jet}(R_{max}, \omega_{min})$ at different impact parameters $b = 3, 8, 13$ fm with fix jet radius $R_{max} = 0.4$ and without acceptance cut ($omega_{min} = 0$). We can see $R_{AA}^{jet}(R_{max}, \omega_{min})$ will go up with increasing impact parameter because of less nuclear medium effect at larger impact parameter, which is similar to R_{AA} for single hadron spectra in Au+Au collisions at $\sqrt{s} = 200$ GeV observed at RHIC. Also $R_{AA}^{jet}(R_{max}, \omega_{min})$ increases with E_T from less than 0.4 to slightly larger than 0.6 in central collisions at $b = 3$ fm.

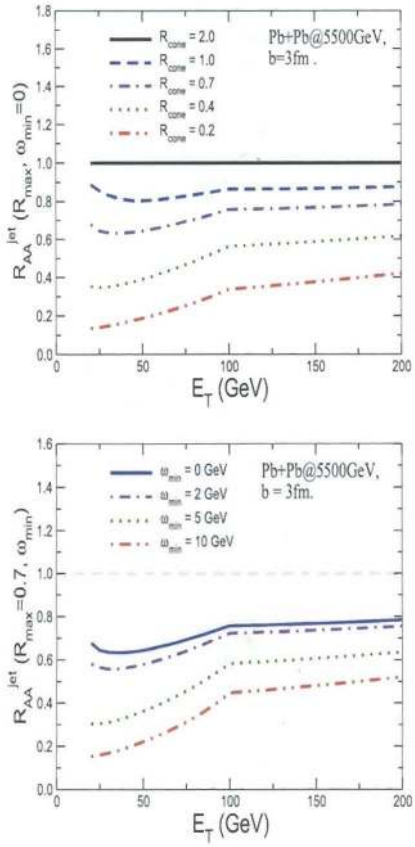

FIG. 8: (Color online) E_T-dependent nuclear modification factor $R_{AA}^{jet}(R_{max}, \omega_{min})$ at different jet cone radius R_{max} (top panel) and at different acceptance cut ω_{min} (bottom panel) at $b = 3$ fm in Pb+Pb collisions with $\sqrt{s} = 5500$ GeV.

In Fig. 8 the evolutions of nuclear modification factor of jet shape are shown by varying the size of jet cone radius R_{max} and detect acceptance cut ω_{min}. From the top panel of Fig. 8 one can observe that by increasing the cone radius R_{max}, the curve of $R_{AA}^{jet}(R_{max}, \omega_{min})$ for all E_T will goes higher and finally reaches to one when $R_{max} = 2.0$. This kind of evolving with jet cone radius results from the fact that the larger the jet cone radius is, the more lost energy of the fast parton should be found inside the jet cone, and when jet cone radius $R_{max} = 2.0$, all lost energy will be inside the cone and we obtain $R_{AA}^{jet}(R_{max} = 2.0, \omega_{min} = 0) = 1.0$. Furthermore, the bottom panel of Fig. 8 shows that $R_{AA}^{jet}(R_{max}, \omega_{min})$ decreases with increasing acceptance cut ω_{min}, due to less energy in the cone with larger acceptance cut. Fig. 8 clearly demonstrates that the quenching of the jet cross sections $R_{AA}^{jet}(R_{max}, \omega_{min})$ depends critically on the choice or R_{max} and ω_{min}. Thus, for the same centrality, E_T and $\sqrt{s}$ the continuum of quenching values is expected to help differentiate between competing models of parton energy loss [29], thereby eliminating the order of magnitude uncertainty in the extraction of the QGP density.

Now we turn to the numerical results on jet shape in Pb+Pb collisions with colliding energy $\sqrt{s} = 5500$ GeV at LHC as illustrated in Fig. 9, Fig. 10 and Fig. 11. From Fig. 9 we can read clearly the dependence of medium-induced jet shapes on the impact parameter, jet energy and cone radius. With the same jet energy and same cone radius, and the different features between jet shape in vacuum and medium-induced jet shape by increasing the impact parameter, the medium-induced jet shape becomes flatter whereas jet shape in vacuum keeps intact because the latter does not have a impact parameter dependence. By decreasing the cone radius from $R = 0.7$ to $R = 0.4$ we also obtain flatter jet shapes. However, we observe that with higher jet energy, both jet shape in vacuum and medium-induced jet shape will become steeper with higher peak at small r/R by comparing figures in the top panel to figures in the bottom panel in Fig. 9, which demonstrates that at higher jet energy, the jet energy distribution in vacuum and medium-induced jet energy distribution are more characterized by soft radiation at small r/R. Furthermore the global property that medium-induced jet shapes are always found to be much flatter than jet shape in vacuum shows the large angle gluon radiation in medium are more favorable than that vacuum.

In Fig. 10 jet shape in vacuum, medium-induced jet shape and total jet shape with different cone radii and different jet energies in Pb+Pb collisions with $\sqrt{s} = 5500$ GeV are illustrated together for comparison. An interesting conclusion by reading this figure is there is no very large difference between jet shape in vacuum and the total jet shape in heavy-ion collisions. The underlining reason for this surprising results is although medium-induced gluon radiation may broaden the jet shape a little bit, this kind of effect may be offset by the effect of jet energy shifting to higher value due to energy loss as compared to the case without energy loss(in vacuum), which should result in steeper jet shape because jet shape at higher energy becomes much steeper, as shown in previous discussions. By shortening jet cone radius from $R = 0.7$ to $R = 0.4$ we see a larger difference between jet shape in vacuum and the total jet shape in medium, which can be easily understood from the fact that by decreasing jet cone radius, less energy carried away by radiated gluon will be inside the jet cone, and thus the effect due to jet quenching will be more pronounced than the one with larger cone radius.

To demonstrate more clearly the difference of jet shape in vacuum and the total jet shape in heavy-ion collisions in Pb+Pb collisions at LHC, we plot in Fig. 11 the ratios of the total jet shape in heavy-ion collisions to jet shape in vacuum with several jet energies $E_T = 20, 50, 100, 200$ GeV for different jet cone radii at impact parameter $b = 3$ fm in Pb+Pb collisions at LHC. In the small $r/R < 0.25$ region, our model of leading-

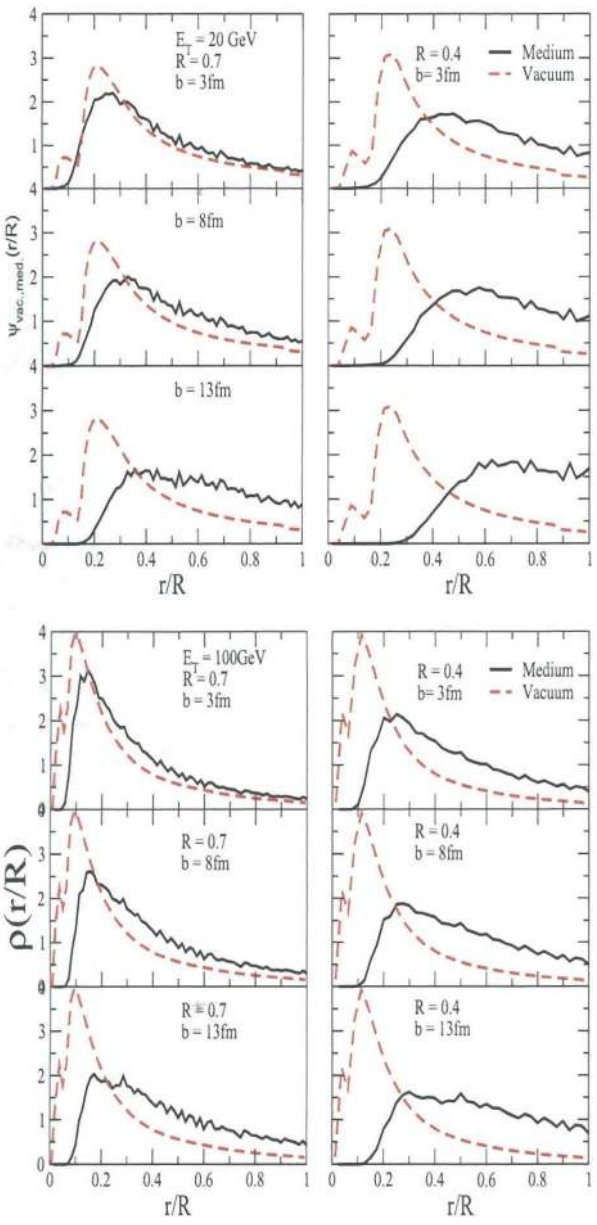

FIG. 9: (Color online) Jet shape in vacuum and medium-induced jet shape for jet energy at 20 GeV (top panel) and 100 GeV (bottom panel) at different impact parameters in Pb+Pb collisions at LHC.

order calculation with Sudakov resummation and non-perturbative contribution will be less reliable because in this region, soft and collinear radiation will dominate and next-to-leading order corrections should be noticeable. In large $r/R > 0.25$ region our model gives excellent descriptions for data at Fermilab in Run II (CDF II) as shown in Fig. 1 and in our discussion will focus on this region only. Fig. 11 shows at $0.25 < r/R < 0.5$, the ratio of the

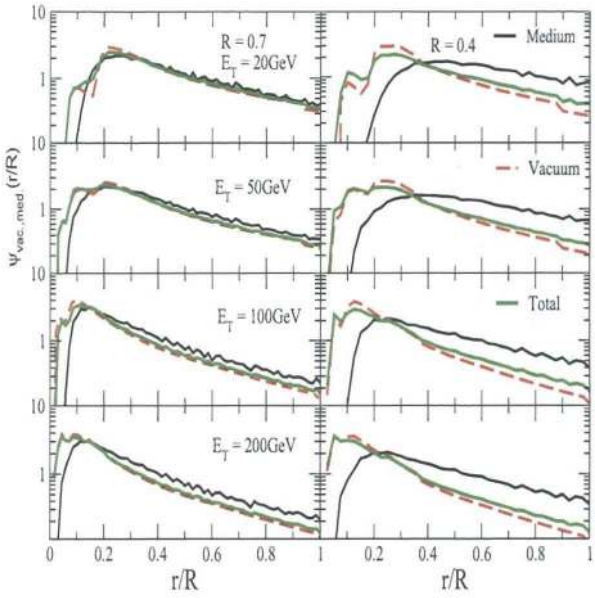

FIG. 10: (Color online) Comparisons of jet shape in vacuum, medium-induced jet shape, and total jet shape with cone radius $R = 0.7$ and cone radius $R = 0.4$ for different jet energies $E_T = 20, 50, 100, 200$ GeV respectively in Pb+Pb collisions at LHC.

total jet shape in heavy-ion collisions to jet shape in vacuum is smaller than one, while when r/R is larger than 0.5, the ratio is larger than one. As we discussed previously, the deviation of the ratio from unity will be more obvious with smaller jet cone radius ($R = 0.4$) where less radiated energy will be included in the jet cone. With cone radius $R = 0.4$, the ratio could reach about 1.5 when $r/R \to 1$. However, to observe this large enhancement at $r/R > 0.5$ at experiments very high resolution in experimental measurements should be needed.

V. CONCLUSION

Acknowledgments

We thank M. H. Seymour for helpful discussion. This research is supported by the US Department of Energy, Office of Science, under Contract No. DE-AC52-06NA25396 and in part by the LDRD program at LANL, the NNSF of China and the MOE of China under Project No. IRT0624.

APPENDIX A: JET CROSS SECTIONS

In this paper we focus exclusively on large momentum transfer processes, $p_T^2 \gg \Lambda^2_{\rm QCD}$, that can be systematically calculated in the framework of a reliable theory, the perturbative QCD factorization approach. Factorization

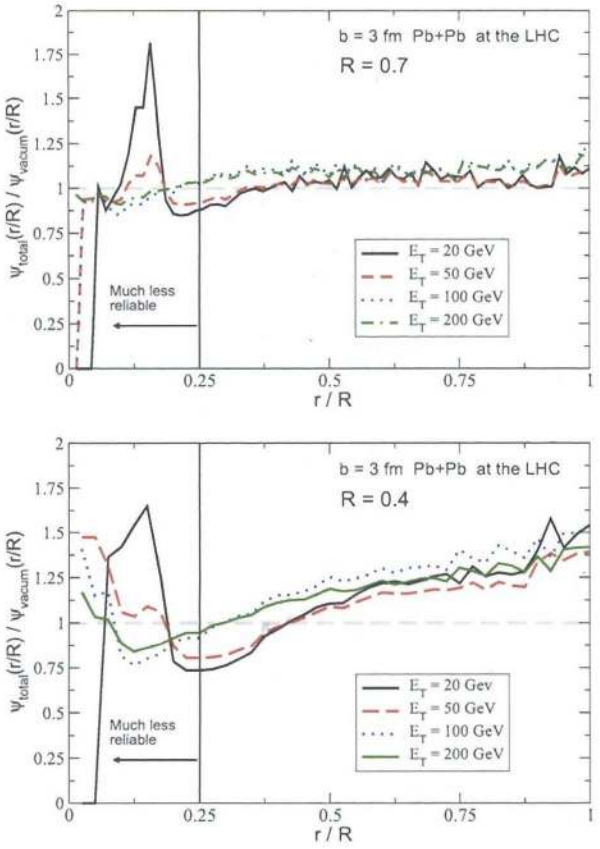

FIG. 11: (Color online) The ratios of total jet shape in heavy-ion collisions to jet shape in vacuum with jet energies $E_T = 20, 50, 100, 200$ GeV for cone radius $R = 0.7$ (top panel) and cone radius $R = 0.4$ (bottom panel) at $b = 3$ fm in Pb+Pb collision with $\sqrt{s} = 5500$ GeV.

not only separates the short- and long-distance QCD dynamics but implies universality of the parton distribution functions (PDFs) and fragmentation functions (FFs) and infrared safety of the hard scattering cross sections. For hadronic collisions, one of the most inclusive processes is jet production. To lowest order (LO) the invariant differential cross section reads [19]:

$$\frac{d\sigma_{h_a h_b}}{dy_c d^2p_{T_c}} = K \sum_{abcd} \int_{y_{d\,\min}}^{y_{d\,\max}} dy_d \frac{\phi_{a/h_a}(x_a,\mu_f)\phi_{b/h_b}(x_b,\mu_f)}{x_a x_b} \times \frac{\alpha_s^2(\mu_r)}{s^2} |\overline{M}_{ab\to cd}|^2 \,. \quad \text{(A1)}$$

Here, $s = (P_a + P_b)^2$ is the squared center of mass energy of the hadronic collision and $x_a = p_a^+/P_a^+$, $x_b = p_b^-/P_b^-$ are the lightcone momentum fractions of the incoming partons. In this formulation, for massless initial-state quarks and gluons,

$$y_{d\,\max(\min)} = +(-)\ln\left(\frac{\sqrt{s}}{m_{T\,d}} - \frac{m_{T\,c}}{m_{T\,d}} e^{+(-)y_c}\right) , \quad \text{(A2)}$$

where $m_{T_i}^2 = m_i^2 + p_{T_i}^2$. In Eq. (A1) $\phi_{i/h_i}(x_i, \mu_{f\,i})$ is the distribution function of parton "i" in the hadron h_i and μ_r and $\mu_{f\,i}$ are the renormalization and factorization and scales, respectively. In this work calculations are done strictly in the collinear factorization approach and we use the CTEQ6.1 LO PDFs [20]. $|\overline{M}_{ab\to cd}|^2$ are the squared matrix elements for $ab \to cd$ partonic sub-processes.

Numerical results for inclusive jet cross sections in high energy hadronic collisions are shown in Fig. 12. The top panel compares the LO calculation, Eq. (A1), to CDF data on jet cross sections in $\mathrm{p} + \bar{\mathrm{p}}$ at $\sqrt{s} = 1.96$ TeV. Excellent agreement between data and the theory using $K = 1.5$, independently extracted from the charged hadron $h^+ + h^-$ differential cross section at the Tevatron. It indicates $\sim 50\%$ next-to-leading order correction. Alternatively, we have studied the sensitivity of the cross section to the choice of the factorization and renormalization scales $\mu_r = \mu_f = p_T/2$ and $2p_T$. Not surprisingly, the uncertainty is also on the order of $\sim 50\%$, similar to the phenomenological K-factor. Jet shapes depend on the parton species, quarks versus gluons, and the insert shows the fraction of quark jets versus p_T at the Tevatron. The bottom panel gives predictions for the corresponding jet cross sections at the LHC for $\sqrt{s} = 14$ TeV and 5.5 TeV, without quenching. Insert shows the increased fraction of gluon jets relative to the Tevatron.

We can now evaluate the feasibility of jet shape measurements at the LHC. During the first three years of running, even at a fraction of the designed $\mathcal{L} = 10^{34}$ cm^{-2}s^{-1}, LHC is expected to deliver an integrated luminosity of 10 fb^{-1} per year. In heavy ion collisions, nominal $\mathcal{L} = 10^{27}$ cm^{-2}s^{-1} is not expected to be achieved either. An integrated luminosity of 1 nb^{-1} per year is a realistic projection. The anticipated quenching factor for energetic jets is two to four, $R_{AA} = 0.25 - 0.5$ [18, 22]. Taking this into account but neglecting for the moment the complications associated with jet reconstruction in the high particle multiplicity environment of heavy ion collisions, from Fig. 12 we find that excellent $< 10\%$ statistical precision can be achieved for inclusive measurements of jets of p_T as high as 160 GeV in Pb+Pb reactions and 1.3 TeV in p+p reactions. Jet *shape* measurements require higher statistics since the shape functions are precipitously falling as of $r/R \to 1$. We expect that very good, $< 30\%$ at large $r/R \sim 1$, *jet shape* measurements will be possible to p_T as high as 100 GeV and 900 GeV in Pb+Pb and p+p collisions, respectively.

With this motivation we proceed to the theory of jet shapes in the vacuum and the strongly-interacting partonic medium which we anticipate will become the next as opposed to a repetition of the program at RHIC.

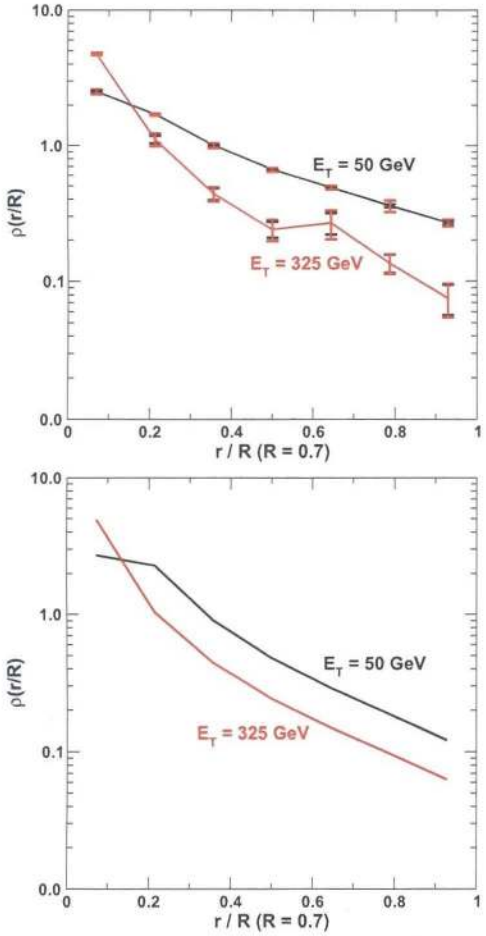

FIG. 14: Caption

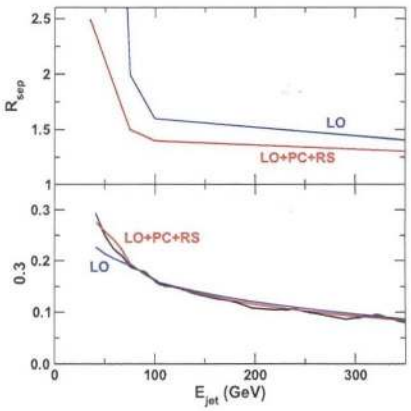

FIG. 15: Caption

[1] X. N. Wang and M. Gyulassy, Phys. Rev. Lett. **68**, 1480 (1992).

[2] M. Gyulassy, I. Vitev, X. N. Wang and B. W. Zhang, arXiv:nucl-th/0302077.

[3] R. Baier, Y. L. Dokshitzer, A. H. Mueller, S. Peigne and D. Schiff, Nucl. Phys. B **484**, 265 (1997) [arXiv:hep-ph/9608322]; B. G. Zakharov, JETP Lett. **63**, 952 (1996) [arXiv:hep-ph/9607440]; N. Armesto, C. A. Salgado and U. A. Wiedemann, Phys. Rev. Lett. **94**, 022002 (2005) [arXiv:hep-ph/0407018].

[4] M. Gyulassy, P. Levai and I. Vitev, Nucl. Phys. B **594**, 371 (2001) [arXiv:nucl-th/0006010]; M. Gyulassy, P. Levai and I. Vitev, Phys. Lett. B **538**, 282 (2002) [arXiv:nucl-th/0112071].

[5] X. N. Wang and X. F. Guo, Nucl. Phys. A **696**, 788 (2001) [arXiv:hep-ph/0102230]; B. W. Zhang and X. N. Wang, Nucl. Phys. A **720**, 429 (2003) [arXiv:hep-ph/0301195]; A. Majumder, E. Wang and X. N. Wang, Phys. Rev. Lett. **99**, 152301 (2007) [arXiv:nucl-th/0412061].

[6] P. Arnold, G. D. Moore and L. G. Yaffe, JHEP **0111**, 057 (2001) [arXiv:hep-ph/0109064]; P. Arnold, G. D. Moore and L. G. Yaffe, JHEP **0011**, 001 (2000) [arXiv:hep-ph/0010177].

[7] A. Adare *et al.* [PHENIX Collaboration], Phys. Rev. C **77**, 064907 (2008) [arXiv:0801.1665 [nucl-ex]].

[8] S. A. Bass, C. Gale, A. Majumder, C. Nonaka, G. Y. Qin, T. Renk and J. Ruppert, arXiv:0808.0908 [nucl-th].

[9] Proceedings of Quark Matter 2008 at Jaipur, India, February 4-10, 2008.

[10] J. Collins and J. W. Qiu, Phys. Rev. D **75**, 114014 (2007) [arXiv:0705.2141 [hep-ph]].

[11] D. G. . d'Enterria *et al.* [CMS Collaboration], J. Phys. G **34**, 2307 (2007).

[12] M. H. Seymour, Nucl. Phys. B **513**, 269 (1998) [arXiv:hep-ph/9707338].

[13] S. D. Ellis, J. Huston, K. Hatakeyama, P. Loch and M. Tonnesmann, Prog. Part. Nucl. Phys. **60**, 484 (2008) [arXiv:0712.2447 [hep-ph]].

[14] Y. L. Dokshitzer and B. R. Webber, Phys. Lett. B **352**, 451 (1995) [arXiv:hep-ph/9504219].

[15] C. S. Fischer and R. Alkofer, Phys. Lett. B **536**, 177 (2002) [arXiv:hep-ph/0202202].

[16] M. Klasen and G. Kramer, Phys. Rev. D **56**, 2702 (1997)

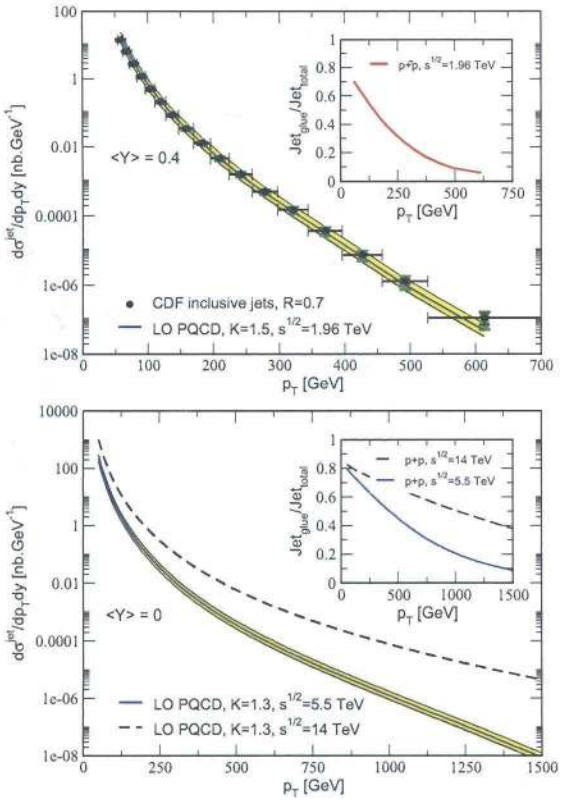

FIG. 12: Top panel: Inclusive jet cross section in p+$\bar{\text{p}}$ collisions at the Tevatron $\sqrt{s} = 1.96$ GeV calculated to LO in PQCD and compared to the CDF run II data [21]. Insert shows the fraction of gluon jets as a function of p_T. Bottom panel: predicted baseline jet cross sections in p+p collisions at the LHC at $\sqrt{s} = 5.5$ TeV and 14 TeV.

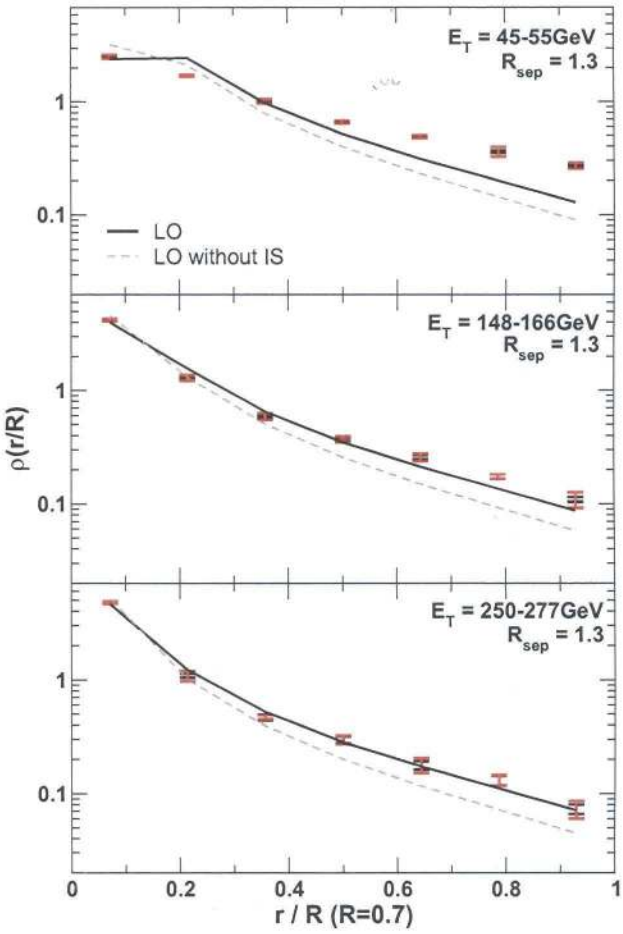

FIG. 13: Caption

APPENDIX B: JET SHAPE AND R_{sep}

A simple calculation with only leading-order contribution gives a decent interpretation of high p_T jet shape data. The R_{sep} parameter is often taken as 'free', here we will start with $R_{sep} = 1.3$. In Fig. 13, we can see the good description of high p_T data, and also the decreasing accuracy as the momentum is decreased. We can also see the necessity of including the initial state radiation, especially for the larger angles relative to the jet axis.

Hence, leading order splitting (with a caveat of the use of a fit R_{sep}) provides a good description of Tevatron jet shape data above $\sim 200GeV$, with decreasing applicability below this. The inherent problem is that the Tevatron jets alter in shape as you decrease the energy. However, the LO treatment only moves the line up or down (except for the zeroth bin that changes to adjust the normalization - see fig ()): the only energy dependence in the LO splitting calculation is in the scale of the coupling. We need to include further physics that has an energy dependence.

One solution is to use the R_{sep} parameter as variable - to fit the results at lower energies by increasing this from 1.3. However, this is not a very physical solution. The obvious deficiency in our treatment so far is the neglect of higher orders. We shall see that the inclusion of some of these higher order effects works in the right direction, but does not remove the need for a momentum dependent R_{sep}.

A convenient method of fitting R_{sep} to the data is to fit the data in fig () of ref (): the total of the jet within $r = 0.3$ of the jet axis. The resulting shape will follow from this. In fig (), we show the result of the fit below and the R_{sep} parameters above. At high energies, we settle at $R_{sep} = 1.3$ as used above; at lower momenta R_{sep} needs to be increased.

As we go below $\approx 75GeV$, it is impossible to fit the width data using LO only, even with a variable R_{sep}.

[arXiv:hep-ph/9701247].
[17] D. E. Acosta *et al.* [CDF Collaboration], Phys. Rev. D **71**, 112002 (2005) [arXiv:hep-ex/0505013].
[18] I. Vitev, Phys. Lett. B **639**, 38 (2006) [arXiv:hep-ph/0603010].
[19] I. Vitev, J. T. Goldman, M. B. Johnson and J. W. Qiu, Phys. Rev. D **74**, 054010 (2006).
[20] J. Pumplin, D. R. Stump, J. Huston, H. L. Lai, P. Nadolsky and W. K. Tung, JHEP **0207**, 012 (2002).
[21] A. Abulencia *et al.* [CDF II Collaboration], Phys. Rev. Lett. **96**, 122001 (2006).
[22] S. Wicks and M. Gyulassy, J. Phys. G **34**, S989 (2007).
[23] I. Vitev, Phys. Rev. C **75**, 064906 (2007) [arXiv:hep-ph/0703002].
[24] M. Djordjevic and M. Gyulassy, Nucl. Phys. A **733**, 265 (2004) [arXiv:nucl-th/0310076].
[25] I. Vitev, Phys. Lett. B **630**, 78 (2005) [arXiv:hep-ph/0501255].
[26] I. Vitev, arXiv:0806.0003 [hep-ph].
[27] M. Gyulassy, P. Levai and I. Vitev, Phys. Rev. Lett. **85**, 5535 (2000) [arXiv:nucl-th/0005032].
[28] M. Gyulassy, I. Vitev, X. N. Wang and P. Huovinen, Phys. Lett. B **526**, 301 (2002).
[29] A. Majumder, J. Phys. G **34**, S377 (2007) [arXiv:nucl-th/0702066].
[30] S. Wicks, arXiv:0804.4704 [nucl-th].
[31] T. Sjostrand, S. Mrenna and P. Skands, JHEP **0605**, 026 (2006) [arXiv:hep-ph/0603175].
[32] C. Markert, R. Bellwied and I. Vitev, arXiv:0807.1509 [nucl-th].
[33] This condition allows for the deflection of the jet and can be seen to the finite rapidity range $0 < y_g < y_{\rm jet}$ for the emitted gluon